Knowl. Manag. Aquat. Ecosyst. 2026, 427, 8
© D. Philpott *et al.*, Published by EDP Sciences 2026
https://doi.org/10.1051/kmae/2026002

www.kmae-journal.org

Knowledge & Management of Aquatic Ecosystems

Journal fully supported by Office français de la biodiversité

RESEARCH PAPER OPEN ACCESS

Large-scale spatial analyses reveal hotspots of proliferative kidney disease in brown trout and interactive effects of temperature and parasite load

Duncan Philpott[1,*], Joacim Näslund[1], Serena Donadi[1], Max Lindmark[2] and Anti Vasemägi[1,3,*]

[1] Swedish University of Agricultural Sciences, Department of Aquatic Resources, Institute of Freshwater Research, Stångholmsvägen 2, SE178 93 Drottningholm
[2] Swedish University of Agricultural Sciences, Department of Aquatic Resources, Institute of Marine Research, Turistgatan 5, SE-453 30 Lysekil
[3] Chair of Aquaculture, Estonian University of Life Sciences, Kreutzwaldi 46a, 51014 Tartu, Estonia

Received: 21 October 2025 / Accepted: 8 January 2026

Abstract – Proliferative kidney disease (PKD) poses a threat to wild salmonids, yet its spatial patterns remain poorly understood, particularly at large scales and across varied ecosystems. We combined the largest nationwide screening of brown trout (*Salmo trutta*), consisting of 1072 fish from 155 locations, spanning a 1480 km latitudinal gradient, with process-based stream-temperature modelling. From this data, we map infection by the parasite *Tetracapsuloides bryosalmonae (T.b)*, quantify parasite load (using qPCR from kidney tissue), and calculate renal hyperplasia across Sweden under different thermal regimes. PKD emerged if study-period mean water temperatures approached a threshold of approximately 15.4 °C and renal hyperplasia peaked near 17 °C; however, warm water did not always cause disease: asymptomatic individuals were common above the temperature threshold. Spatial mixed-effects models revealed that parasite load and temperature interacted to determine disease severity, whereby severe PKD was associated with lower parasite loads under warmer conditions. Furthermore, deviations from broad latitudinal patterns were observed, where distinct coastal hotspots in central Sweden would be overlooked by assuming a simple temperature-driven latitudinal gradient. Our model shows that such patterns remain after accounting for temperature and parasite load, indicating that local conditions and additional environmental drivers are likely affecting epidemiology at relatively small spatial scales. Management actions that moderate stream temperatures, such as riparian shading or the removal of impoundments, or reduce suitable habitat for bryozoan hosts, may therefore mitigate disease impacts under a warming climate.

Keywords: PKD / *Tetracapsuloides bryosalmonae* / emerging disease / climate impacts / *Salmo trutta* / temperature dependence / spatial clustering / process-based temperature models / spatial mixed-effects modelling

1 Introduction

Under the current trajectory of climate change, aquatic species are becoming increasingly vulnerable to emerging diseases (Marcogliese, 2008; McCullough *et al.*, 2009; Reid *et al.*, 2019). Among salmonids, proliferative kidney disease (PKD) represents a significant emerging threat. First described by Roberts and Shepherd (1974), PKD is characterised by pronounced renal hyperplasia and is caused by the myxozoan parasite *Tetracapsuloides bryosalmonae* (Canning *et al.*, 1998). The parasite has a complex two-host life cycle, using freshwater bryozoans as its primary host and salmonid fish as intermediate hosts. Infection of a compatible salmonid enables the parasite's transmission back to bryozoa, through the fish's urine, completing the life cycle and spreading the parasite throughout the river (Morris and Adams, 2006).

For *T. bryosalmonae* infections to cause PKD, elevated water temperatures are required. Laboratory experiments as early as 1986 indicated that the minimum temperature required for parasite infection can be as low as 9°C in rainbow trout (*Oncorhynchus mykiss*) (Clifton-Hadley *et al.*, 1986; Gay *et al.*, 2001). However, the temperature threshold for PKD development, following parasite infection, ranges from 12°C to 15°C with symptoms intensifying under warmer thermal regimes (Morris *et al.*, 2005; Bettge *et al.*, 2009; Strepparava *et al.*, 2018), leading to higher mortality rates (Waldner *et al.*, 2021). Young-of-the-year (YoY) fish are most vulnerable to PKD, but any fish that has not previously been considered

*Corresponding authors: duncan.philpott@slu.se; anti.vasemagi@slu.se

susceptible (Ferguson and Ball, 1979). Subsequently, adult fish that have survived previous disease are remarked as "immune" to PKD symptoms whilst remaining a host of *T. bryosalmonae* (Klontz *et al.*, 1986). Beyond the laboratory, PKD development may be influenced by additional ecological and environmental factors beyond temperature alone, such as low levels of dissolved oxygen increasing the susceptibility of fish to diseases in general (Wang *et al.*, 2023) and high nutrient loads enhancing primary host habitat (Hartikainen *et al.*, 2009).

PKD has been extensively researched in wild rivers and lakes across Europe and North America (Seagrave *et al.*, 1981; MacConnell and Peterson, 1992; Sterud *et al.*, 2007; Wahli *et al.*, 2002; Kristmundsson *et al.*, 2010; Dash and Vasemägi, 2014; Lewisch *et al.*, 2018; Lauringson *et al.*, 2022). However, research aiming to advance the understanding of PKD epidemiology with respect to real-world temperatures is often limited by resources. In-stream water temperature observations are often/mainly restricted to limited spatial scales featuring a single catchment, climate or region (Bruneaux *et al.*, 2017; Lauringson *et al.*, 2021; Debes *et al.*, 2017; Schmidt-Posthaus *et al.*, 2015, 2017; Rubin *et al.*, 2019). However, the consideration of small spatial scales limits the understanding of *T. bryosalmonae* presence, infection prevalence and disease severity across different climates and geographies. When spatial scales are larger, in-stream temperature measurements are often substituted for air temperature or altitude as a proxy (Ros *et al.*, 2021; Wahli *et al.*, 2008). Yet since in-stream temperature can vary greatly at small spatial scales due to heat exchange processes such as cool groundwater input, or variation in riparian vegetation that can offer shade from solar radiation (Caissie, 2006), such proxies can be inaccurate.

One alternative to increase the accuracy of a temperature proxy without the use of temperature loggers is process-based temperature modelling. Process-based models can simulate energy exchanges with many heating or cooling inputs with a resolution that ranges from global grids (van Vliet *et al.*, 2012; Wanders *et al.*, 2019) to river reach scales (Bartholow, 1989). Notably, at the reach scale, in-stream water predictions can be a stark improvement over air temperature proxies (Ficklin *et al.*, 2012). One such model, used within the focal country of this study (Sweden), is S-HYPE, which is a semi-distributed model developed and maintained by the Swedish Meteorological and Hydrological Institute (Lindström *et al.*, 2010), building on the widely used HBV (Bergström *et al.*, 1976; Lindström *et al.*, 1997). S-HYPE provides robust river flow, nutrient and temperature predictions at a sub-catchment scale.

The Swedish Veterinary Institute (SVA) confirmed the first presence of *T. bryosalmonae* in Sweden in 2008, with infections identified in both Atlantic salmon (*Salmo salar*) and brown trout (*Salmo trutta*) at six of the thirteen locations screened in the counties of Jämtland and Västerbotten (Alfjorden and Hellström, 2008). The extent of *T. bryosalmonae* distribution in Swedish waters beyond these regions remains unknown, yet observations of *T. bryosalmonae* in northernmost Norway (Lauringson *et al.*, 2022) suggest that parasite presence is not latitudinally limited by temperature and could be expected nationally. Since river temperatures in the south of Sweden are comparable to those of many central European rivers, severe cases of PKD could be expected, while many northern rivers may remain too cold for PKD to develop. Regional analyses show that the Swedish climate is warming, and snow cover days are reducing (Graham *et al.*, 2007; Schimanke *et al.*, 2022), posing a potential threat to cold-water-adapted species such as the brown trout in regions where river temperatures are reduced by snowmelt input.

The broad range of thermal regimes across Swedish waterways provides an ideal opportunity to study the complex interactions between *T.b*, PKD pathology and temperature, on brown trout across a broad ecological scale. By combining large-scale parasite screening and disease assessment with process-based in-stream temperature models, this study aims to determine the spatial distribution of *T. bryosalmonae* and the severity of PKD in wild Swedish brown trout populations whilst assessing how the differing temperature regimes may influence PKD development with respect to disease pathology and parasite intensity.

2 Materials and methods

2.1 Sample collection

Young-of-the-year (YoY) brown trout were sampled during 2022 and 2023 using standardised wading electrofishing in coordination with the Swedish national fish monitoring program from sites spanning a 1480 km latitudinal gradient in a 358,000 km^2 region. Approximately 10 fish were sampled per site unless, in infrequent circumstances, it was deemed a risk to the local population. Subsequently, the median number of lethally sampled fish per site was 7 (SD: 3.2, Range 1-15). Sampling windows were determined by the Swedish survey window for standardised electrofishing (late summer and autumn), which is suitable given the knowledge that renal hyperplasia should be evident following multiple months of elevated water temperatures (Strepparava *et al.*, 2020). In 2022, 863 fish were sampled from 129 locations with a mean sampling day of 29-Aug-2022 (SD: 16.3). In 2023, 209 fish were sampled from 32 locations with a mean sampling day of 29-Aug-2023 (SD: 17.7) (Fig. 1). In total, 155 unique sites across 105 rivers were sampled at altitudes ranging from 1 m to 605 m, with river sizes varying from <1 m to 40 m wet width (data recorded by individuals conducting the electrofishing and stored in the Swedish Electrofishing Register database, https://www.slu.se/elfiskeregistret/).

2.2 Renal hyperplasia and parasite load estimation

Renal hyperplasia was calculated as the residuals of the measurement of kidney cross-sectional area from a model of expected uninfected kidney cross-sectional area given fish length (for YoY brown trout) (Philpott *et al.*, 2025). To determine the parasite load in *T. bryosalmonae*-infected individuals, a TaqMan real-time qPCR assay targeted a 91 bp fragment of the *T. bryosalmonae* 18S rRNA gene with the primers PKX18s1266-f1426r and a PKX18s_1399 probe (both developed by Hutchins *et al.*, 2018) in a 10 µL reaction comprising HOT FIREPol Probe qPCR Mix Plus, primers and probe at 100 pmol/µL, and 3 µL of DNA template (20 ng/µL), run on a Bio-Rad CFX384 Touch with a two-step protocol (12 min at 95 °C, then 40 cycles of 95 °C denaturation and 60 °C annealing/plate read). The starting quantity (formula 1) of

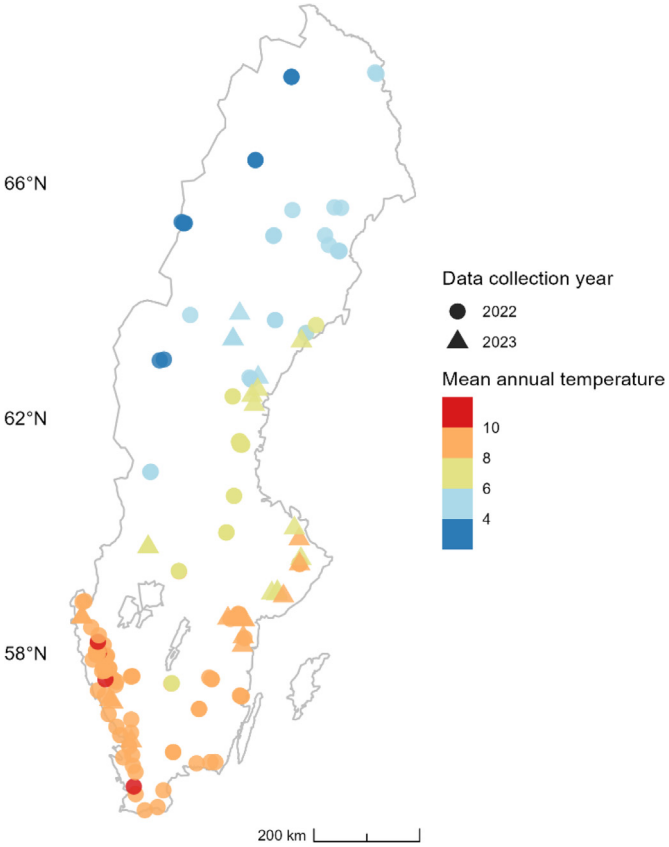

Fig. 1. Study area and sampling year of the 155 sites coloured by mean annual water temperature as retrieved from S-HYPE for the relevant sampling year.

parasite DNA was calculated by the use of plate-specific standard curves produced from a synthetic PKX standard dilution series spanning five 10-fold dilutions. Curves were calculated across the fourteen plates to assess inter-assay, and each sample was analysed in three technical replicates to ensure robust quantification. The mean starting quantity across three technical replicates of each sample was used in this study:

$$Starting\ Quantity = 10^{\frac{C_t - b}{m}} \quad (1)$$

Where C_t is the threshold cycle value, m is the slope of the standard curve, and b is the intercept of the standard curve. Seventy-five individuals from the 2022 collection were excluded from renal hyperplasia calculation due to a lack of reported body length at capture. These samples were still included in analyses concerning parasite load and temperature.

Additional details concerning sample dissection, measurement, kidney size modelling and preservative adjustment can be found in the method paper by Philpott *et al.* (2025).

2.3 Temperature data

Due to the broad spatial extent of the study area, modelled water temperature values from the Swedish-HYPE model (S-HYPE; Lindström *et al.*, 2010) version 5_27_0 were used to ensure full geographical and temporal data coverage. Study point data and S-HYPE sub-catchments (derived from SVAR2022 vector, Swedish Meteorological and Hydrological Institute (SMHI, 2025)) were spatially joined by intersection using a GIS, ArcGIS Pro version 3.2.0 (Esri Inc., Redlands, CA) to obtain subcatchment identifiers for each site (median catchment size: 13 km^2, min: 0.2 km^2, max: 90 km^2. Subcatchment sizes varied with respect to complexity). In the S-HYPE model areas, the temperature values are calculated at the outflow point of the sub-catchment. A manual validation of each site and associated temperature calculation point was performed in the GIS, and subsequent reallocation of twelve study sites was performed where more hydrologically suitable sub-catchments were available. For instance, when a point intersected a subcatchment close to its upstream limit, the next upstream subcatchment was selected to ensure the minimum distance between subcatchment outflow and the study site, whilst improving hydrological similarity between the temperature calculation point and site location. The temperature data from the matched sub-catchments were retrieved at daily resolution for each data year (Fig. 1).

Additional long-term temperature data, matching 57 sites, was retrieved from the Miljödata MVM database (SLU, 2023). These data were spatially joined with a 200-m search radius and watercourse name validation. Thirty years of S-HYPE modelled temperatures were compared against real-world monthly samples to verify model accuracy (supplementary material S1).

Comparison with long-term MVM observations revealed abnormal residuals for one site (Norrhultsbäcken); therefore, it was excluded from the temperature-dependent analyses since it transpired that the stream received flush water from a wastewater treatment plant, which is not accounted for in the S-HYPE processes.

The large span of latitudes across the study area and different sampling dates required unique temperature windows for each location. The temperature window from which mean temperature statistics were derived began once a 5-day rolling mean exceeded 12 °C and ended upon the sampling of the fish. The choice of 12 °C mirrors the coldest temperatures employed in laboratory infection studies (of brown trout) by Bailey *et al.* (2017), whereby parasite load is still demonstrated to increase. Furthermore, 12 °C ensured all sites were included since some of the mountain streams fed by snowmelt did not reach 15 °C water temperature.

2.4 Spatial statistics

Global spatial autocorrelation of prevalence, renal hyperplasia and parasite load attributes was assessed with Moran's *I* statistic (Moran, 1950) using a permutation test within the *spdep* package (Bivand *et al.*, 2002) using 9,999 random permutations. The test compares the calculated Moran's *I* against random permutations of the attribute values (while maintaining the spatial structure) to determine if the result differs significantly from the null hypothesis that the data is randomly spread. Weights were calculated using 10 k-nearest neighbours and an adaptive Gaussian kernel to account for the uneven sampling efforts (median kernel size: 111 km, 90th percentile: 352 km; the number of neighbours was determined

by sensitivity analysis, indicating stable results when choosing between 8 and 12 neighbours).

For the identification of hot spots, cold spots and outliers, local indicators of spatial association were calculated with Local Moran's I (Anselin, 1995). The calculation was performed using the *rgeoda* package (Li *et al.*, 2025). Clusters were extracted and mapped at three significance intervals: $0.05 \geq p > 0.01$, $0.01 \geq p > 0.001$, and $p < 0.001$.

2.5 Bayesian change point analysis

Change point analysis was conducted with the R package mcp (Lindeløv, 2024) to identify a mean temperature window associated with renal hyperplasia. Such an approach allows for the modelling of changes in both the mean and the variance of the residuals, which provides flexibility to account for the large number of infected but asymptomatic fish (subclinical infections) across the range of temperatures in the dataset.

A two-segment model (*i.e.*, single change point) was fitted. A constant mean was specified across the range of temperatures before the change insertion after: (formula 2), such that kidney size is expected to remain constant under non-stressful temperature regimes. After the change (formula 2), both the mean (*i.e.*, linear trend) and residual variance are free to change (formula 3). An uninformative prior for the change point of uniform probability across the range of temperature values was used.

Before the change point:

$$y_t = \beta_0 + \varepsilon_t,\ \varepsilon_t \sim N(0, \sigma_0^2). \tag{2}$$

After the change point:

$$y_t = \beta_1 + \beta_2 \mathrm{T}_t + \varepsilon_t,\ \varepsilon_t \sim N(0, \sigma_1^2), \tag{3}$$

where y_t = renal hyperplasia$_t$, T_t = mean study-period site temperature$_t$. Posterior distributions of the change-point parameter were obtained from Markov Chain Monte Carlo (MCMC) sampling, and both the posterior mean and 95% credible interval were extracted to estimate the change point and uncertainty of the threshold. The plots of the posterior densities and model fit were used to assess convergence and fit quality (supplementary material).

2.6 Spatial mixed-effects modelling

To quantify the effects of temperature and parasite load on renal hyperplasia whilst accounting for site-level replication and spatial autocorrelation, we fitted a spatial generalised linear mixed model using the *sdmTMB* package (Anderson *et al.*, 2023). Renal hyperplasia was rescaled to strictly positive values and modelled using a Gamma distribution with a log link function, which is well-suited for skewed continuous response variables with variance increasing with the mean.

In consideration of the thermal threshold identified by the changepoint analysis, temperature values were split into a baseline linear term and an additional slope above the threshold in a "hockey-stick" fashion. This was done by creating a new temperature variable (T^+), where temperatures below a threshold were set to zero. The fixed effects included temperature terms, *T. bryosalmonae* load and their interaction, permitting the effect of parasite load on renal hyperplasia to vary with temperature. The interaction of temperature and parasite load was permitted through the full range of temperature values since bryozoan growth and densities are not subject to the same thermal threshold. All of the covariates were scaled by subtracting the mean and dividing by the standard deviation to ease model fitting and interpretation of coefficients. We let the intercept vary by sampling site to account for unmeasured local effects and non-independence among samples collected from the same location. In addition to these site-level random effects, we included spatial random effects, representing a spatially correlated latent process. We assumed these spatial random effects to be drawn from a Gaussian Markov random field, constrained by Matérn covariance functions. The SPDE approach (Lindgren *et al.*, 2011) requires a triangulated mesh, which we constructed with a 5 km cutoff between vertices using the function fm_rcdt_2d_inla() from the *fmesher* R package (Lindgren 2023), ensuring the estimated spatial correlation range was at least three times this minimum distance.

The final model was specified for an individual fish sampled at site g, where the expected renal hyperplasia μ_g was described as:

$$\eta_s = \beta_0 + \beta_1 T + \beta_2 T^+ + \beta_3 L + \beta_4 (T \times L) + b_g + \omega_s, \tag{4}$$

$$\mu_s = \exp(\eta_s), \tag{5}$$

$$\mathbb{E}(y_s) = \mu_s, \tag{6}$$

where $y_{s,t}$ is the response (renal hyperplasia) at location s, η is the linear predictor in link space, μ_s is the conditional mean, $\beta_{0,\ldots,4}$ are coefficients for variables temperature (T), temperature above the threshold of 15.45 °C (T^+), load (L) and the interaction between load and temperature, respectively. Site-specific random deviations from the overall intercept are denoted b_g, and ω_s represent a Gaussian Markov random field, where $\omega_s \sim \mathrm{MVN}(0,\ \Sigma_{\omega_s})$.

2.7 Data analysis and visualisation

All statistical and spatial analyses were performed in R version 4.4.1 (R Core Team 2024). Summary site-level statistics were derived from individual-level data for both *T. bryosalmonae* presence and prevalence, mean renal hyperplasia and mean parasite load. Only the sites with confirmed *T. bryosalmonae* presence were used in subsequent analyses for renal hyperplasia and parasite load.

Spatial objects visualising the distributions of *T. bryosalmonae* presence, renal hyperplasia, prevalence and parasite load were prepared using the *sf* package (Pebesma, 2018). Data cleaning, rearrangement and visualisation of graphical, tabular, time series and spatial data were performed using the *tidyverse, table1, zoo, ggspatial, spdep* and *patchwork* set of R packages (Wickham *et al.*, 2019; Rich, 2023; Pedersen, 2025; Zeileis *et al.*, 2025; Bivand *et al.*, 2002).

Table 1. Individual-level qPCR and phenotypic results.

Individual-level data	*T.b* absent ($N = 633$)	*T.b* present ($N = 292$)	PKD ($N = 147$)	Overall ($N = 1072$)
Parasite load (starting quantity of DNA)				
Mean (SD)	NA (NA)	57000 (151000)	137000 (427000)	83700 (278000)
Median [Min, Max]	NA [NA, NA]	10500 [7.52, 1320000]	42700 [13.6, 4740000]	17100 [7.52, 4740000]
Missing	633 (100%)			633 (59.0%)
Renal hyperplasia (mm^2)				
Mean (SD)	0.0848 (0.406)	0.418 (0.472)	3.90 (2.96)	0.739 (1.80)
Median [Min, Max]	0.0451 [−1.21, 1.94]	0.370 [−0.784, 1.29]	2.89 [1.32, 17.8]	0.216 [−1.21, 17.8]
Missing	42 (6.6%)	46 (10.5%)		88 (8.2%)

Table 2. Population-level temperature model data and prevalence.

Population-level data	*T.b* absent (N = 72)	*T.b* present (N = 46)	PKD (N = 37)	Overall (N = 155)
Mean study period temperature (°C)				
Mean (SD)	15.7 (2.36)	16.8 (2.09)	17.4 (0.778)	16.3 (2.28)
Median [Min, Max]	16.2 [8.06, 19.6]	17.1 [8.16, 20.8]	17.3 [15.7, 19.5]	16.9 [8.06, 20.8]
Mean yearly water temperature (°C)				
Mean (SD)	7.59 (1.68)	9.18 (1.76)	9.75 (0.797)	8.44 (1.89)
Median [Min, Max]	7.14 [3.55, 10.6]	9.63 [3.74, 11.6]	9.88 [7.79, 11.3]	8.99 [3.55, 11.6]
Prevalence				
Mean (SD)	NA (NA)	54.9 (36.9)	91.3 (17.5)	71.1 (34.8)
Median [Min, Max]	NA [NA, NA]	50 [9.09, 100]	100 [20.0, 100]	90 [9.09, 100
Missing	72 (100%)			72 (46.5%)

3 Results

3.1 Detection of *T. bryosalmonae*, calculated renal hyperplasia, parasite load, and site prevalence

Of the 1072 individuals screened using qPCR for *T. bryosalmonae*, 439 were infected by the parasite (Tab. 1). Renal hyperplasia peaked at a score of 17.8 mm^2, and proliferative kidney disease (clinical infection) occurred at a renal hyperplasia score >1.3 mm^2 (kidney scores greater than the 99th percentile of uninfected fish)(Fig. 2b). Following this definition, 154 individuals in this study were afflicted with PKD.

Parasite loads ranged from 7.5 copies of parasite DNA to 4740000 copies. (assay limit of quantification, LoQ was 18 copies per reaction, effective limit of detection, LoD = 2.8 copies over three technical replicates (Philpott *et al.*, 2025)). Seven samples were below LoQ but above LoD.

At the population-level, uninfected and infected locations spanned similar temperature ranges (Tab. 2); however, sites with *T. bryosalmonae* present had slightly higher mean study-period temperature (16.8 °C) than uninfected locations (15.7 °C), while sites with PKD symptoms were considerably higher (17.4 °C). Furthermore, this trend persisted across mean annual temperatures; lowest at *T. bryosalmonae* absent sites (7.6 °C), higher at *T. bryosalmonae* present sites (9.2 °C), and highest at PKD sites (9.8 °C). Prevalence differed substantially between populations with *T. bryosalmonae* present, 54.9% (SD 36.9), and the populations with visible PKD symptoms, 91.3% (SD 17.5). Generally, at sites where *T. bryosalmonae* was present, prevalence frequently approached 100% (Fig. 2a) with a single infected individual occasionally found in an otherwise healthy location (*i.e.*, prevalence values ranging 0–25%).

3.2 Spatial distribution of parasite presence, prevalence, renal hyperplasia and parasite load

T. bryosalmonae was detected across a broad latitudinal range, with presence decreasing from south to north (Fig. 3a). Most sites in southern and south-western Sweden contained infected trout, yet differences in parasite presence occurred in as little as 0.5 km range. Infected fish were also detected at the northernmost and high-altitude sites (in western Sweden).

Infection prevalence varied strongly at small spatial scales (Fig. 3b). Although 100% prevalence was observed even in northern populations, high prevalence occurred more frequently in the south, and sharp contrasts between neighbouring sites reduced spatial autocorrelation.

Severe renal hyperplasia was concentrated in coastal streams in southern and south-western Sweden (Fig. 3d), with the river Loån (60°N, east coast) exhibiting the most extreme cases. Northern sites were largely unaffected, with renal hyperplasia detected at only one location (Fig. 3d).

Parasite load also declined with latitude (Fig. 3c), though the lowest observed loads still occurred within southern Sweden. The highest parasite loads generally coincide in similar regions to the severest examples of renal hyperplasia, for example, along the southern Swedish coastlines.

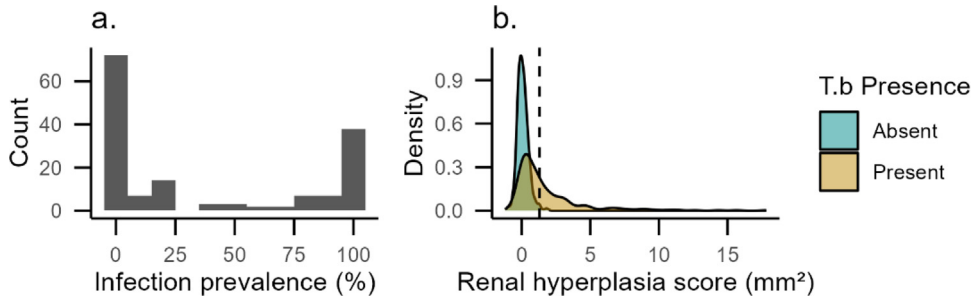

Fig. 2. a. Histogram of infection prevalence counts across the 155 locations. **b.** distributions of the densities of renal hyperplasia grouped by infection status. The threshold for symptomatic fish, score = 1.3, is marked with a dashed horizontal line.

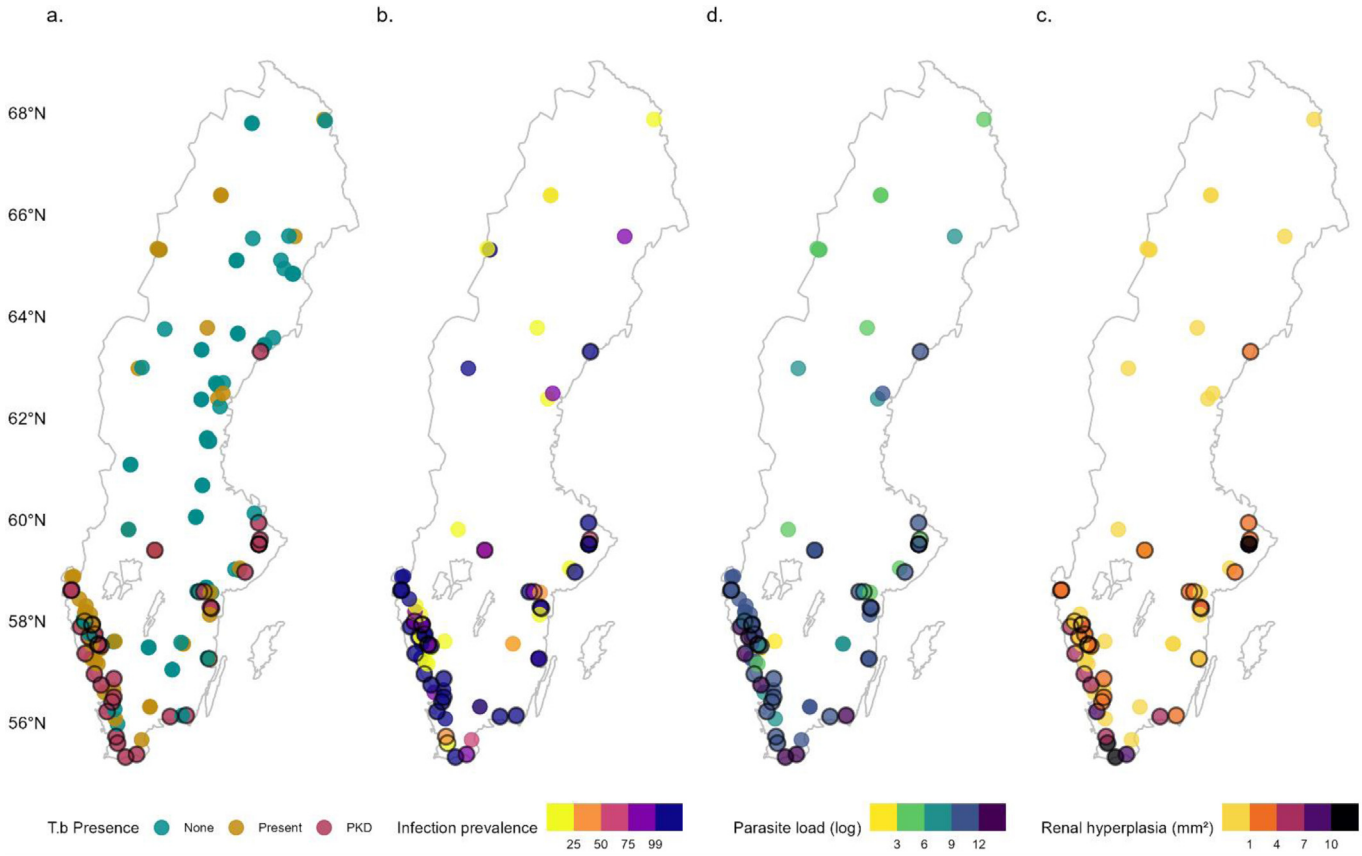

Fig. 3. Maps depicting the spatial distribution of **a.** *T. bryosalmonae* infection (present depicts locations with infection, but with subclinical infections), **b.** site infection prevalence, **c.** mean parasite load (log-transformed) and **d.** maximum renal hyperplasia. Individual-level data has been grouped and displayed as a single site point. Populations with PKD are circled in black.

3.3 Spatial autocorrelation, hot spots and cold spots of prevalence, parasite load and renal hyperplasia

Global Moran's *I* showed significant spatial autocorrelation for two of the three variables tested (Tab. 3). Prevalence values did not differ significantly from the random expectations, indicating that the proportion of individuals infected at a site varied independently of its location. Instead, maximum renal hyperplasia demonstrated a signal of spatial dependence, indicating that populations with severe disease symptoms tend to occur close to each other, for example, across multiple neighbouring catchments, as opposed to being randomly distributed throughout Sweden. Similarly, parasite loads were also positively autocorrelated, yet with a weaker signal, suggesting similar spatial structure but with greater variance.

Despite 100% infection prevalence being regularly observed, neighbouring locations often featured considerable variation, and local indications of spatial association (LISA) revealed limited clustering overall (Fig. 4a). Three statistically significant high-high clusters (hotspots) were identified in the southern extent of the west coast, while a few significant low-low clusters (cold spots) are scattered sparsely throughout the country.

Table 3. Global Moran's *I* statistics for spatial autocorrelation of infection prevalence, parasite load and renal hyperplasia. Observed Moran's *I* values were calculated using an adaptive Gaussian kernel with 10 nearest neighbours. Significance was assessed by Monte Carlo permutation tests (9,999 permutations), with *p*-values reported as Permutation *p*-value.

Variable	Observed Moran's I	Permutation *p*-value
Prevalence	−0.005	0.0373
Parasite Load (log transformed population mean)	0.119	0.01
Renal hyperplasia (maximum)	0.189	0.001

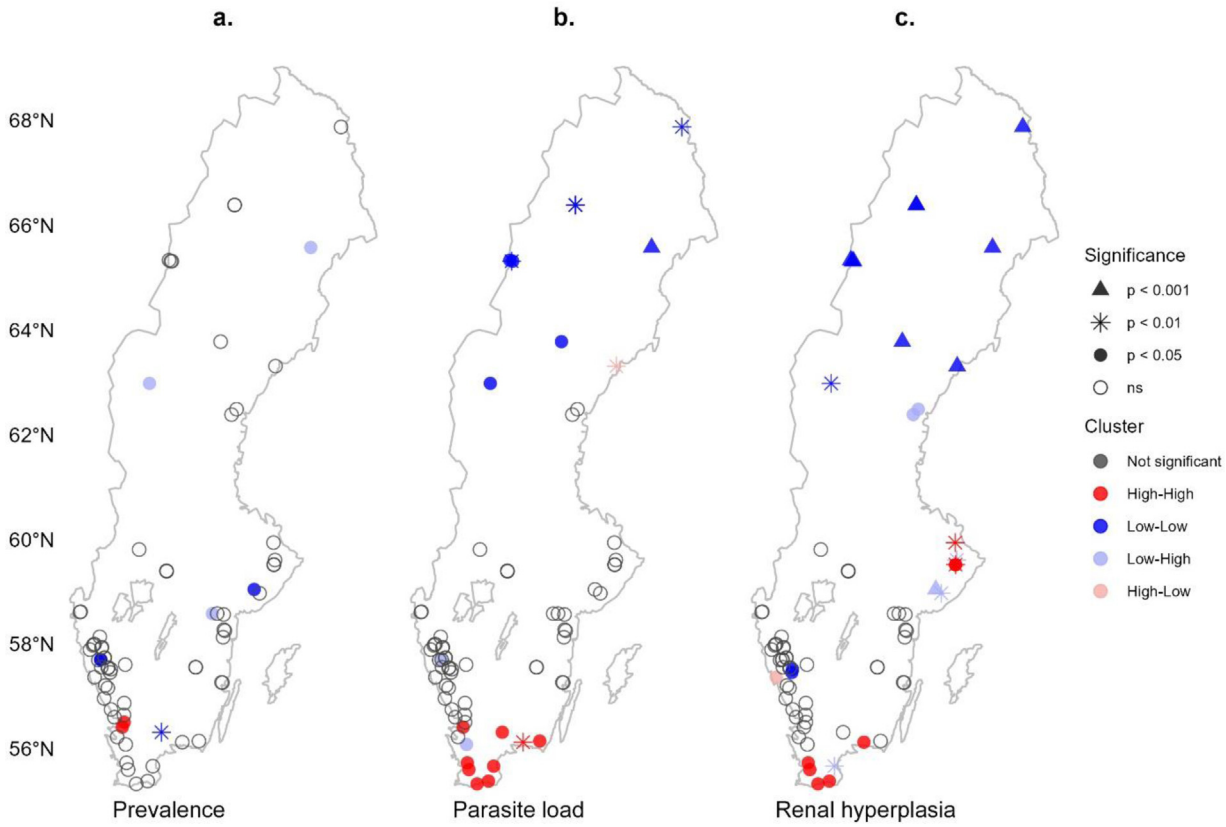

Fig. 4. Local indicators of spatial autocorrelation for the standardised variables representing **a.** population infection prevalence, **b.** mean parasite load and **c.** maximum renal hyperplasia. Spatial weights were defined with an adaptive Gaussian kernel (see Methods). For each variable, LISA statistics were computed using 9,999 complete permutations. Colours designate cluster type while symbols encode permutation significance levels. Cluster assignment used a 0.05 cutoff for significance.

Parasite load exhibited clearer latitudinal structure, with distinct hot-spot clusters in the south and cold spots in the north (Fig. 4b). The single location with PKD in the north was a statistically significant high-low outlier representing high parasite loads in a low parasite load neighbourhood. Conversely, one site in the very south of the country was identified as a low-high outlier with significantly lower parasite loads than its neighbours. Overall, the hotspots and cold spots are relatively uniform, suggesting a regional-level process responsible for determining parasite loads.

Clinical PKD clustered in the south of Sweden (Fig. 4c). These clusters did not always align with parasite load, as parasite load hotspots were more spatially extensive. In mid-Sweden, hotspots of renal hyperplasia occurred in areas where parasite loads were not significantly clustered. This apparent mismatch likely reflects that site-level summary statistics used for LISA mask substantial within-site variation, such that parasite load may explain disease severity among individuals within populations, while broader spatial contrasts in maximum renal hyperplasia between sites are influenced by additional environmental drivers. In this region, the response is strongly polarised: infected fish either exhibit severe renal hyperplasia or remain largely asymptomatic.

3.4 Modelled water temperatures

Modelled daily water temperatures highlighted consistent warming and cooling behaviours across the range of sites

Table 4. Changepoint model fit.

Parameter	Estimate	95% CrI	$\text{Pl}\hat{R}$	*Effective sample size*
Temperature threshold (changepoint)	15.45	[15.09, 15.80]	1	1986
β_0(*Intercept before changepo* int)	0.19	[0.03, 0.34]	1	8106
β_1(*Intercept after changepo* int)	1.09	[0.41, 1.73]	1	831
β_2 (*Temperature coefficient*)	0.64	[0.21, 1.10]	1	1047
σ_1(var *iance before changepo* int)	0.44	[0.32, 0.56]	1	3963
σ_2(var *iance after changepo* int)	2.53	[2.34, 2.71]	1	9408

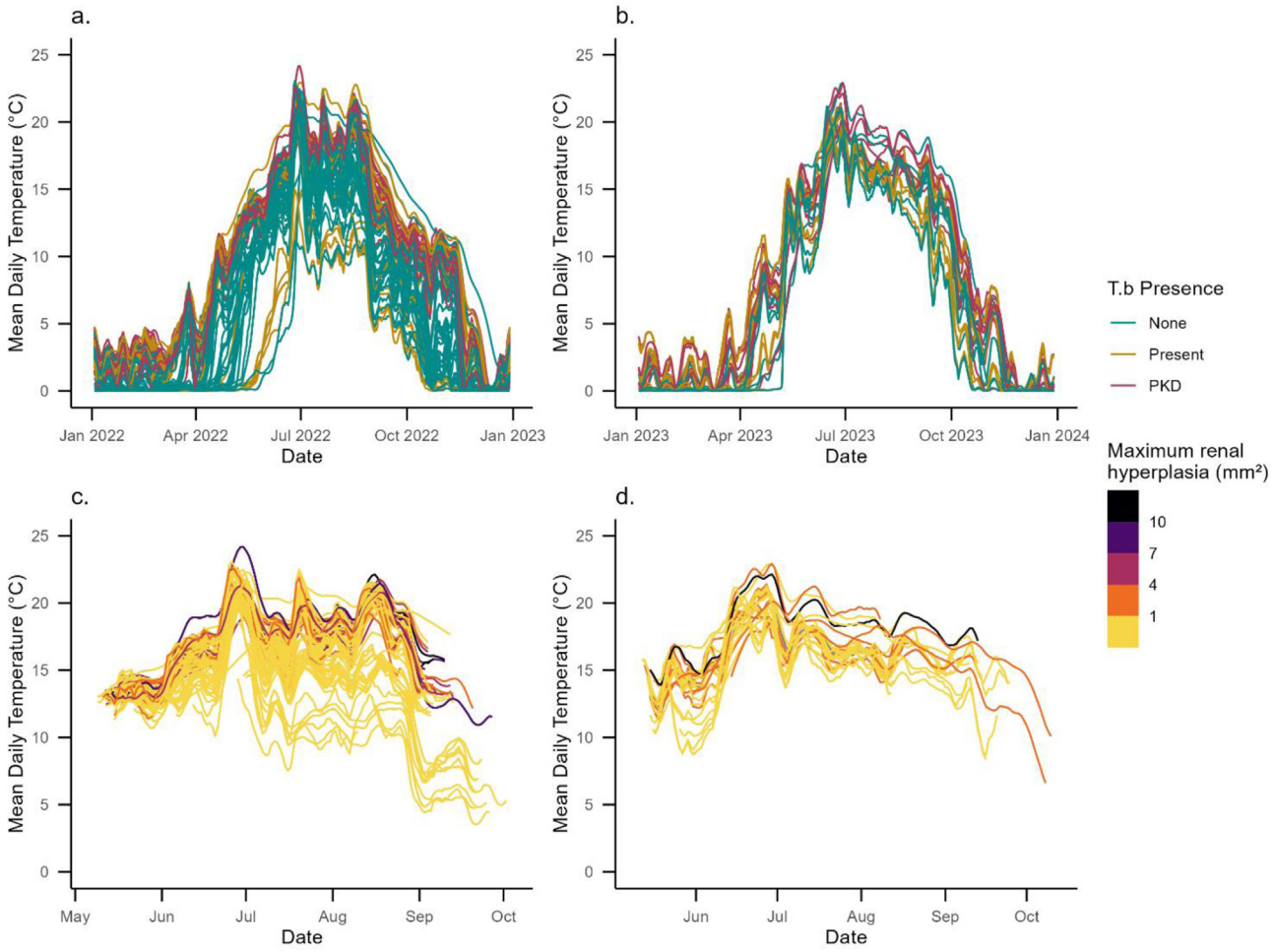

Fig. 5. Mean modelled daily water temperature values with colours designated by parasite presence (**a**-**b**) and maximum renal hyperplasia (**c**-**d**), yellow lines represent fish without pathological symptoms. Locations sampled in 2022 are shown in (**a**,**c**), and locations sampled in 2023 are shown in (**b**,**d**).

throughout the year, with peak temperatures achieved for all locations at similar times (Figs. 5a and 5b). The model demonstrates a broad overlap in the temperatures of both infected and uninfected sites, yet the locations with PKD symptoms are generally hotter throughout the year (Figs. 5c and 5d). In the 2022 data, except for locations subjected to meltwater runoff, all of the locations reached temperatures suitable for the development of PKD at a similar time; however, the temperatures increasingly varied as the summer progressed. In 2023, there was much less variance in temperatures. Furthermore, lower peak temperatures are demonstrated, yet a longer sustained temperature window, *e.g.*, much warmer September and October in comparison to 2022. In 2022, a site with extreme symptoms achieved the maximum peak water temperature of the dataset at 24°C. PKD symptoms were still detectable in our latest sampling that occurred in October 2023,

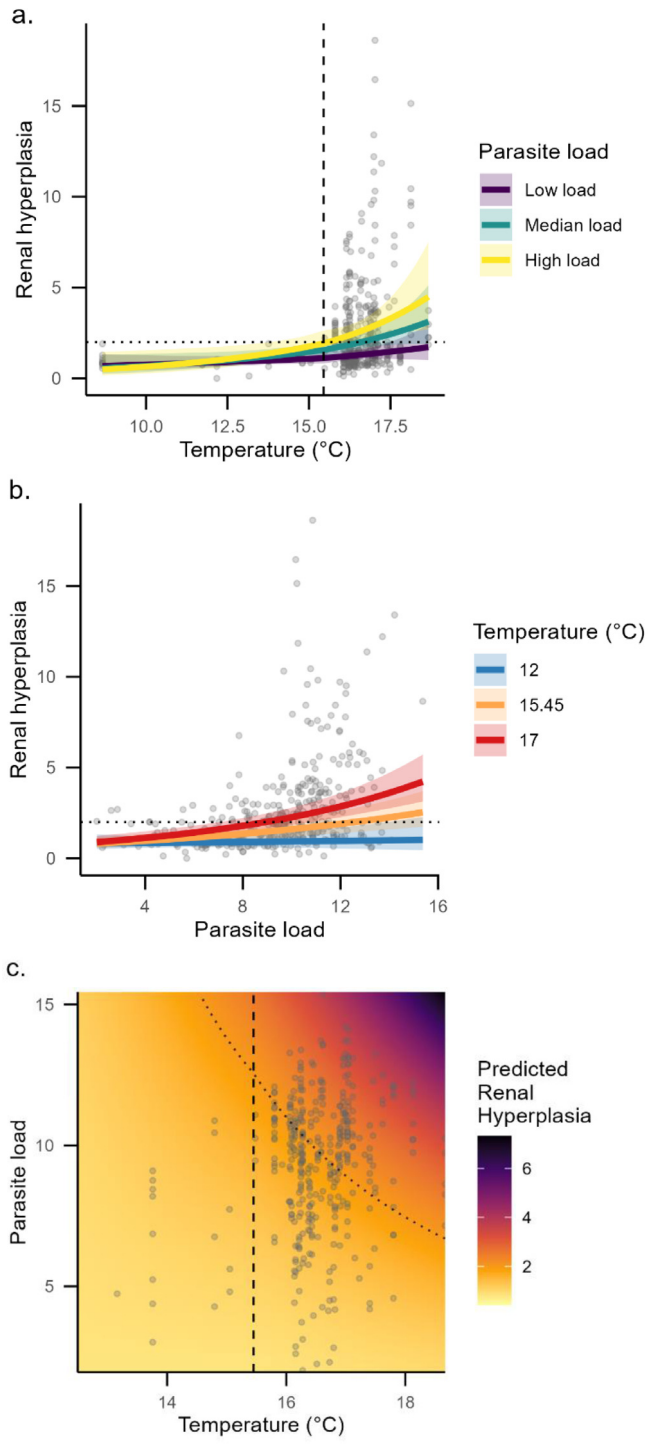

Fig. 6. Plots showing **a.** Predicted renal hyperplasia increases with temperature, with steeper responses at higher parasite loads, indicating that warming disproportionately amplifies pathology in heavily infected fish. **b**. Predicted renal hyperplasia increases with parasite load, and this effect strengthens at higher temperatures, while remaining weak under cooler conditions (no PKD symptoms). **c.** The interaction surface shows that the highest predicted renal hyperplasia occurs where elevated temperatures and high parasite loads coincide; the original data points are shown in grey. Ribbons in a, b represent a 95% confidence interval and across all panels, the dashed line resembles the temperature threshold, and the dotted line resembles the threshold for PKD.

where water temperatures had dropped to as low as 6°C. Lastly, there are warm sites where *T. bryosalmonae* is present; however, we do not observe renal hyperplasia.

3.5 A temperature threshold for PKD in rivers

The temperature threshold required for renal hyperplasia was identified by Bayesian change point analysis as approximately 15.4 °C (95% credible interval: 15.1–15.8 °C) (Tab. 4) for the study-period temperature window, *i.e.*, beginning once water temperatures have crossed 12 °C until the sampling of the fish. Maximum renal hyperplasia scores increased with temperature, and at 17 °C, the greatest renal hyperplasia scores were observed. However, asymptomatic individuals are observed across the temperature range up to 18.6 °C. The biological relevance of the temperature coefficient in the variance-segmented changepoint analysis is skewed by the number of asymptomatic fish upon a linear fit.

3.6 Contributions of parasite load and temperature to renal hyperplasia

Spatial mixed effects modelling revealed that renal hyperplasia increased with both temperature and parasite load, where elevated parasite loads showed the strongest and most consistent association with severe symptoms (predictor estimates, supplementary information Tab. S3). Across the study temperatures, higher parasite loads were associated with higher predicted renal hyperplasia once the temperature threshold was met, and this relationship steepened at warmer temperatures, indicating a significant temperature and parasite load interaction (Fig. 6).

The predicted response surface illustrated that the highest levels of renal hyperplasia occurred under combined high temperature and high parasite load, whereas elevated temperature alone was associated with relatively modest increases in pathology and remained subclinical when parasite load remained low. This pattern indicates that temperature primarily modulates the strength of the parasite pathology relationship rather than acting as an independent driver of severe renal hyperplasia.

Spatial random effects revealed clear spatial structure not captured by covariates or site-level random effects, with a Matérn correlation range of approximately 41 km and a spatial standard deviation of 0.39. This indicated considerable spatial structuring in renal hyperplasia that was not explained by temperature and parasite load alone and is indicative of additional environmental disease drivers.

The weak correlation between temperature and parasite load ($r = 0.31$) suggests these factors largely operate independently, though temperature-dependent ecological processes may influence both parasite infection dynamics and renal hyperplasia.

4 Discussion

4.1 Do elevated water temperatures inevitably lead to proliferative kidney disease?

Our nationwide screening, paired with process-based temperature modelling, indicates that warm water is required

for PKD but, crucially, does not guarantee renal hyperplasia. PKD pathology rose sharply once mean temperatures reached and exceeded 15.4 °C, and the highest renal hyperplasia scores occurred at 17 °C. Yet, even above this threshold, subclinical infections were common, and several warm yet infected sites showed little to no pathology. Spatial mixed-effects modelling indicates that parasite load contributes more to clinical PKD, while elevated temperatures appear to modify the severity of renal hyperplasia rather than acting as the sole driver. Furthermore, the contribution of spatial random effects to the model suggests that local conditions influence disease severity, helping to explain why proliferative kidney disease is not observed across the full range of warm, infected sites.

Under laboratory conditions, it is shown that differing initial parasite loads resulted in different trajectories of disease development. Higher initial parasite loads result in faster onset of symptoms, longer durations of observable pathology and greater variance in recovery times (*i.e.*, the time needed for the kidney to return to a normal size), whereas lower loads lead to greater initial variance in pathology and shorter recovery times (Strepparava *et al.*, 2020). However, increased temperature can reduce the time for clinical infections and prolong recovery times (Strepparava *et al.*, 2020; Bailey *et al.*, 2018). In rivers, the temperature threshold of 15.5 °C coincides with the observed increase in *T. bryosalmonae* and bryozoan eDNA, suggesting increased growth, abundance or activity in the parasite and bryozoans (Mercier *et al.*, 2025).

We sampled fish from locations that exceeded the observed temperature threshold and that were afflicted with high parasite loads, yet still demonstrated minimal renal hyperplasia or completely subclinical infection. Such variance in renal hyperplasia despite high loads and warm water conditions is previously documented both in the wild (Ahmad *et al.*, 2020; Lauringson *et al.*, 2021) and under laboratory conditions. Even in controlled experiments, there is a large variance of renal hyperplasia, and asymptomatic fish have been observed in 16 °C treatments throughout the duration of experiments (Bettge *et al.*, 2009; Bailey *et al.*, 2015; Waldner *et al.*, 2021).

Within populations, heterogeneity in parasite load itself may arise from fish possessing heritable genetic resistance to T. bryosalmonae infection (Debes *et al.*, 2017). However, this mechanism primarily explains individuals with low parasite burdens, whereas the cases observed here involve high parasite loads accompanied by limited pathological response, which is more consistent with variation in host tolerance rather than resistance. Debes *et al.* further emphasised that disentangling genetic tolerance from environmental and random effects requires very large sample sizes, often in the order of thousands of individuals, which exceeds the practicality of field-based studies. Variation in renal proliferation may also be explained by fish movement to thermal refugia during peak temperature events, thus buffering the temperature effects upon renal proliferation and parasite dynamics, as demonstrated by Oexle *et al.* (2025). Fish may subsequently return to sampling sites once water temperatures have declined to more favourable levels, which is often the case at the time of sampling. This may result in the co-occurrence of asymptomatic and clinically affected individuals. Alternatively, severely affected fish may be displaced from their normal habitat if maintaining swimming position becomes energetically costly due to reduced blood haematocrit, leading them to be sampled alongside comparatively healthier individuals (Debes *et al.*, 2017).

Differences in the severity of the worst-affected fish at a given temperature are likely influenced by additional environmental stressors such as eutrophication and urbanisation acting at the ecosystem level (Bailey *et al.*, 2018; Duval *et al.*, 2024). Environmental stressors could increase the physiological stress of the trout (Wang *et al.*, 2023), thereby influencing the hosts' immune response towards *T. bryosalmonae*. In severe cases of proliferative kidney disease, anaemia resulting from impaired renal function (Bruneaux *et al.*, 2017) may further interact with hypoxic habitat conditions, compounding the disease outcomes. Consequently, warm, infected sites where fish remain healthier may indicate good habitat. Identifying additional environmental drivers of PKD in detail would be valuable for disease management and identifying vulnerable populations, as heterogeneity in temperature and other conditions in the wild likely adds further complexity to the development of renal hyperplasia.

4.2 The spatial distribution of *Tetracapsuloides bryosalmonae* in Sweden

The nationwide screening revealed that *T. bryosalmonae*-infected fish are found across the full latitudinal range of the country. Whilst the study of the parasite is generally associated with warmer climates, detection of *T. bryosalmonae* in the northern latitudes was not unexpected and aligns with the findings of studies in cold climate areas such as northern Norway (Lauringson *et al.*, 2022; Mo and Jørgensen, 2017) and Iceland (Kristmundsson *et al.*, 2010). However, the frequency with which *T. bryosalmonae* was detected in mid- to southern Sweden was surprising given that patchy parasite occurrence has been observed at more southern latitudes. Furthermore, the parasite was detected across the entire extent of elevations within our study area despite an expectation for reduced parasite presence at higher elevations (Wahli *et al.*, 2008; Carraro *et al.*, 2017; Ros *et al.*, 2021) and year-round cool streams with snowmelt influence. By contrast, parasite absences are most consistent across regions of production forestry.

The presence of *T. bryosalmonae* is intrinsically linked to the presence of its bryozoan primary hosts, whose distribution is considered to be patchier than the brown trout due to more specific habitat requirements. Bryozoan habitats are positively associated with lentic, nutrient-rich environments (Hartikainen 2009) and can be found in abundance at humic lake mouths (Raddum and Johnsen, 1983; Ricciardi and Reiswig, 1994). Furthermore, PKD-focused research has reported negative bryozoan density trends at higher elevations or steeper stream gradients (Carraro *et al.*, 2017). As a result, suitable bryozoan habitat is likely distributed unevenly across river networks, and in the absence of bryozoans, transmission of *T. bryosalmonae* cannot occur.

Within our national screening, we observed that parasite presence varied at fine spatial scales, consistent with patchy bryozoan habitat expectations. Differences in parasite presence were found between neighbouring small streams within distinct catchments (Kvarsebobäcken and Djupviksbäcken), as close as 2.5 km to each other at 58.6°N on the east coast of

Sweden. While distinct catchments may be expected to differ sufficiently in habitat suitability for bryozoans, such heterogeneity was also observed within a river reach. For example, contrasting parasite presence was observed at 0.5 km (Euclidean distance) in the river Enån north of Sweden's largest lake, Vänern. Extremely fine-scale variability likely reflects the patchy distribution of bryozoan habitat due to differences in stream morphology, whereby substrate or flows limit bryozoan establishment. Comparable fine-scale spatial heterogeneity has also been observed in Estonia and the French Pyrenees (Dash and Vasemägi, 2014; Duval *et al.*, 2024). Such observations of variability in parasite presence could suggest that regional or even catchment-level assessment of the effects of PKD on trout may be hard to capture without a detailed understanding of the mechanisms of primary-host presence and parasite presence.

The abundance of *T. bryosalmonae* infections in diadromous trout populations along the Swedish coastlines echoes the findings of Mo and Jørgensen (2017), where infections were often found in the coastal waters unless the habitat was unsuitable for bryozoans, such as in exceptionally steep and rocky coastal streams. Similarly, the lack of a significant pattern, locally or nationally, in the prevalence of *T. bryosalmonae* in our data could be explained by a mismatch of temperature regimes and bryozoan densities that occur across the diverse range of habitats of the study area, compounded by the movement of fish within the river. Laboratory-based work by Bailey *et al.* (2017) demonstrates that temperature positively influences prevalence, whilst Strepparava *et al.* (2020) highlight that increased initial infection loads can also increase prevalence in the population. In field studies, *T. bryosalmonae* prevalence can be extremely high where rivers are warm and lowland, *e.g.*, mean summer temperatures 20 °C and greater (Debes *et al.*, 2017; Schmidt-Posthaus *et al.*, 2013). Elevation is remarked to moderate this pattern. For example, in Switzerland, Wahli *et al.* (2008) found site-specific prevalences ranging from 2–95%, and Ros *et al.* (2021) reported a negative association between brown trout prevalence and elevation.

4.3 Spatial patterns and trends of parasite load and renal hyperplasia in Sweden

Our analyses reveal statistically significant autocorrelation and local clustering of both parasite load and renal hyperplasia. Hotspots for both were primarily detected in the low-gradient, warm southern rivers, whilst the northern latitudes of Sweden were cold spots. Furthermore, we identified an East Coast hotspot of renal hyperplasia that would be missed by assuming a simple temperature-driven latitudinal gradient. Notably, hotspots for parasite load and for renal hyperplasia did not strictly overlap, but both were broadly governed by temperature. In contrast, the cold spots were highly consistent across both metrics and significant at the highest level.

We also identified significant high–low and low–high outliers. Some likely reflect genuine contrasts where sampling sites are close in Euclidean space but lie in distinct catchments with different thermal regimes and habitats. Therefore, re-analysing with stream-network distances could reduce such artefacts and may strengthen evidence for global autocorrelation. Other outliers may arise from anthropogenic modifications that alter flow regimes, creating lentic conditions and warmer microhabitats (Zaidel *et al.*, 2021). Similar associations between flow modification and thermal conditions have been observed in Estonian ecosystems (Lauringson *et al.*, in press). Coincidentally, our northernmost PKD case occurred downstream of a medium-sized hydropower installation, and the northernmost *T. bryosalmonae* detection was also recorded downstream of a dam; however, no formal association has been investigated. Although dams may create lentic, warmer microhabitats favourable for bryozoans, the small sample size within our dataset does not allow us to directly attribute PKD patterns to dam effects.

When interpreting data on a nationwide scale, within-catchment mechanisms must be considered since renal hyperplasia often increases from headwaters towards lower reaches as water temperatures and suitable primary host habitat improve (Wahli *et al.*, 2008; Carraro *et al.*, 2017; Ros *et al.*, 2021). Within this study, the estimated Matérn range, *i.e.*, where spatial autocorrelation effectively disappears (approximately 41 km), suggests that disease patterns are structured at sub-regional to catchment scales.

The most severe renal hyperplasia was consistently observed along the coastlines where thermally sensitive small streams can regularly experience elevated water temperatures that would perhaps threaten resident trout populations (Donadi *et al.*, 2023). However, the diadromous brown trout that return to these rivers to spawn may continuously repopulate them despite severe PKD.

4.4 Implications for Swedish brown trout

With results from nationwide screening, Swedish fisheries and environmental managers can better understand the threat of acute PKD in Sweden. For example, the numerous small sea-trout streams ranging from southern to mid-Sweden (of which only a fraction were sampled here) appear particularly susceptible to PKD. Notably, negative population trends in these regions have already been identified by Donadi *et al.* (2023).

Confirming that PKD symptoms in wild populations occur when water temperatures exceed 15.5 °C will enable the identification of waterways that may be at risk. Temperature can be monitored or modelled over large spatial scales and is often included in existing monitoring programs. Whilst parasite load information would improve knowledge of ecosystems at risk, the lethal sampling of juvenile trout to quantify parasite load is not feasible for threatened populations or particularly compatible with conservation in general. Therefore, disease monitoring should be as non-invasive as possible. A recent, non-lethal advancement in PKD monitoring, pioneered by Duval *et al.* (2021), provides a reliable method for detecting *T. bryosalmonae* infection using the urine of trout (urine-DNA) and may offer robust quantitative insights into parasite load in the future. Other non-lethal alternatives include sampling of filter-feeding sponges to detect DNA signal from *T. bryosalmonae* (Saks *et al.*, 2026).

Mitigating PKD offers another justification for river restoration focused on both temperature buffering and bryozoan habitat management, as previously highlighted by Ros *et al.* (2021). For example, ensuring sufficient riparian vegetation zones will prevent excessive solar heating of small

streams and mitigate nutrient input (that can drive bryozoan densities) from diffuse sources in agricultural areas (Mayer *et al.*, 2007; Dugdale *et al.*, 2018). Likewise, the removal of small dams (which are abundant and often obsolete throughout Sweden) would reduce impounded water and artificial prime bryozoan habitat (Zaidel *et al.*, 2021).

Finally, the river temperatures we observed have implications beyond PKD. The feeding efficiency of brown trout declines as temperatures exceed 20 °C, with physiological stress increasing rapidly thereafter (Solomon and Lightfoot, 2008), and several of our warmest sites approached (and at times exceeded) these temperatures. Therefore, in the absence of the regular temperature monitoring of rivers in Sweden, process-based temperature models could prove valuable for understanding population trends and locations that can be prioritised for thermal regime management.

5 Conclusion

Our nationwide screening shows that warm water is necessary but not sufficient for developing PKD: symptoms occur around 15.4 °C and peak near 17 °C, yet asymptomatic infections remain common. Both *T. bryosalmonae* infections and thermal regimes that can trigger PKD are relatively commonplace in Sweden. Our spatial model shows that parasite load is a key driver of renal hyperplasia above temperature thresholds, with warm temperatures amplifying parasite effects, but unidentified local environmental drivers are likely also influencing PKD severity.

Broad latitudinal trends are observed for renal hyperplasia and parasite loads, while significant hotspots occur at fine scales in the low-gradient and southernmost extents of the country, where the primary host habitat may be most suitable.

Although parasite load is a key driver of PKD severity, its quantification by lethal sampling of wild fish means that temperature thresholds, such as the one identified in this study, provide a practical tool for identifying ecosystems at increased disease risk. The abundance of PKD and *T. bryosalmonae* infection discovered in this study should highlight the need for targeted disease monitoring and management to mitigate PKD impacts in the Swedish trout population.

Acknowledgments

We would like to acknowledge the anonymous reviewers of this manuscript for their constructive and insightful comments, which motivated additional analyses that improved the overall quality of this manuscript.

Funding

This study was funded by the Swedish Research Council FORMAS grant 2021–01643 (to A.V.).

Data availability statement

The data and core scripts used to perform the analyses in this manuscript are available at the following repository: https://doi.org/10.6084/m9.figshare.30305677.

Supplementary material

Figure. S1. Locations in grey were MVM locations where in-situ temperature data were available, but were not joined to our site data.

Figure. S2. Performance of the model throughout the year across thirty years of data. The points cluster for the excluded site, Norrhultsbäcken, visible in the lower half of the plot, demonstrates where the temperature processes were not captured by SHYPE due to wastewater treatment interference.

Figure. S3. Temperature residuals SMHI modelled water temperatures vs MVM in-situ measurements since 1991, Norrhultsbäcken removed from the dataset.

Figure. S4. Population level data for Renal hyperplasia and parasite load arranged by temperature rank, dashed line indicates the minimum renal hyperplasia score for PKD.

Figure. S5. Scatter plots comparing the variables of **a**. Mean water temperature and renal hyperplasia, coloured by log-transformed parasite load. Uninfected individuals are represented by light grey points. The posterior mean and 95% credible intervals of the first change point are visualised as vertical lines and shaded bands, respectively. **b**. mean parasite load (log-transformed) with within-site infection prevalence, point colour considers the mean water temperature. **c**. Mean water temperature and parasite load (log-transformed) at an individual level, where colour denotes the extent of the individual's renal hyperplasia. **d**. Individual parasite load and renal hyperplasia with mean water temperature indicated by point colour. For a. and d. PKD threshold is illustrated by a dashed horizontal line.

Figure. S6. MCMC chains and density plots for each of the parameters in the mcp changepoint model.

Figure. S7. Spatial random effects from the spatial mixed-effects model of renal hyperplasia. The map shows the estimated spatial random field (ω_s) from the spatial mixed-effects model, representing residual spatial variation in renal hyperplasia after accounting for temperature, parasite load, their interaction, and site-level random effects. Values are shown on the link (log) scale. Positive values (blue) indicate areas where renal hyperplasia is higher than expected based on fixed effects alone, whereas negative values (red) indicate lower-than-expected values.

Table. S1. Summary statistics for temperature residuals between SMHI modelled temperatures and MVM in-situ measurements.

Table. S2. Global Moran's I statistics for spatial autocorrelation of infection prevalence, parasite load and renal hyperplasia. Observed Moran's I values were calculated using an adaptive Gaussian kernel with k nearest neighbours.

Table. S3. Fixed-effect parameter estimates from the spatial mixed effects model explaining renal hyperplasia.Estimates are reported on the link scale. Confidence intervals represent 95% confidence intervals.

The Supplementary Material is available at https://www.kmae-journal.org/10.1051/kmae/2026002/olm.

References

Ahmad F, Debes PV, Nousiainen I, Kahar S, Pukk L, Gross R, Ozerov M, Vasemägi A. 2020. The strength and form of natural selection on transcript abundance in the wild. *Mol Ecol* 30: 2724–2737.

Alfjorden A, Hellström A. 2008. Redovisning av Fiskevårdsmedel för: Pilotprojekt avseende spridning av PKD, proliferativ njurinflammation hos laxfisk till norra Sverige. Uppsala: Swedish Veterinary Agency (SVA).

Anderson SC, Ward EJ, English PA, Barnett LAK, Thorson JT. 2023. sdmTMB: Spatial and Spatiotemporal SPDE-Based GLMMs with 'TMB' (p. 0.8.0). https://doi.org/10.32614/CRAN.package.sdmTMB

Anselin L. 1995. Local indicators of spatial association—LISA. *Geogr Anal* 27: 93–115.

Anselin L. 1995. Local indicators of spatial association—LISA. *Geogr Anal* 27: 93–115.

Bailey C, Rubin A, Strepparava N, Segner H, Rubin J-F, Wahli T. 2018. Do fish get wasted? Assessing the influence of effluents on parasitic infection of wild fish. *PeerJ* 6: e5956.

Bailey C, Schmidt-Posthaus H, Segner H, Wahli T, Strepparava N. 2018. Are brown trout Salmo trutta fario and rainbow trout Oncorhynchus mykiss two of a kind? A comparative study of salmonids to temperature-influenced Tetracapsuloides bryosalmonae infection. *J Fish Dis* 41: Article 2.

Bailey C, Segner H, Casanova-Nakayama A, Wahli T. 2017. Who needs the hotspot? The effect of temperature on the fish host immune response to *Tetracapsuloides bryosalmonae* the causative agent of proliferative kidney disease. *Fish Shellfish Immunol* 63: 424–437.

Bartholow JM. 1989. Stream temperature investigations: field and analytical methods. Instream Flow Information Paper No. 13. U. S. Fish and Wildlife Service Biological Report 89. Washington, DC.: U.S. Fish and Wildlife Service Research and Development.

Bergström S. 1976. Development and application of a conceptual runoff model for scandinavian catchments. SMHI Rapporter: Hydrologi och Oceanografi, 7: 1-134. The Swedish Meteorological and Hydrological Institute (SMHI), Norrköping.

Bettge K, Wahli T, Segner H, Schmidt-Posthaus H. 2009. Proliferative kidney disease in rainbow trout: time- and temperature-related renal pathology and parasite distribution. *Dis Aquat Org* 83: 67–76.

Bivand R. 2002. spdep: Spatial Dependence: Weighting Schemes, Statistics (p. 1.4-1). https://doi.org/10.32614/CRAN.package.spdep

Bruneaux M, Visse M, Gross R, Pukk L, Saks L, Vasemägi A. 2017. Parasite infection and decreased thermal tolerance: Impact of proliferative kidney disease on a wild salmonid fish in the context of climate change. *Funct Ecol* 31: 216–226.

Caissie D. 2006. The thermal regime of rivers: a review. *Freshw Biol* 51: 1389–1406.

Canning EU, Curry A, Feist S, Longshaw M, Okamura B. 1998. *Tetracapsula bryosalmonae* n.sp. For PKX organism, the cause of PKD in Salmonid fish. *Bull Eur Assoc Fish Pathol* 199: 203–206.

Carraro L, Bertuzzo E, Mari L, Fontes I, Hartikainen H, Strepparava N, Schmidt-Posthaus H, Wahli T, Jokela J, Gatto M, Rinaldo A. 2017. Integrated field, laboratory, and theoretical study of PKD spread in a Swiss prealpine river. *Proc Natl Acad Sci* 114: 11992–11997.

Clifton-Hadley RS, Richards RH, Bucke D. 1986. Proliferative kidney disease (PKD) in rainbow trout Salmo gairdneri: further observations on the effects of water temperature. *Aquaculture* 55: 165–171.

Dash M, Vasemägi A. 2014. Proliferative kidney disease (PKD) agent *Tetracapsuloides bryosalmonae* in brown trout populations in Estonia. *Dis Aquat Org* 109: Article 2.

Debes PV, Gross R, Vasemägi A. 2017. Quantitative genetic variation in, and environmental effects on, pathogen resistance and temperature-dependent disease severity in a wild trout. *Am Nat* 190: 244–265.

Donadi S, Näslund J, Sandin L, Sers B, Vasemägi A, Degerman E. 2023. Contrasting long-term trends in juvenile abundance of a widespread cold-water salmonid along a latitudinal gradient: effects of climate, stream size and migration strategy. *Ecography* 2023: e06522.

Dugdale SJ, Malcolm IA, Kantola K, Hannah DM. 2018. Stream temperature under contrasting riparian forest cover: Understanding thermal dynamics and heat exchange processes. *Sci Total Environ* 610–611: 1375–1389.

Duval E, Blanchet S, Quéméré E, Jacquin L, Veyssière C, Lautraite A, Garmendia L, Yotte A, Parthuisot N, Côte J, Loot G. 2021. Urine DNA (uDNA) as a non-lethal method for endoparasite biomonitoring: Development and validation. *Environ DNA* 3: Article 5.

Duval E, Blanchet S, Quéméré E, Jacquin L, Veyssière C, Loot G. 2024. When does a parasite become a disease? eDNA unravels complex host-pathogen dynamics across environmental stress gradients in wild salmonid populations. *Sci Total Environ* 946: 174367.

Ferguson HW, Ball HJ. 1979. Epidemiological aspects of proliferative kidney disease amongst rainbow trout *Salmo gairdneri* Richardson in Northern Ireland. *J Fish Dis* 2: 219–225.

Ficklin DL, Luo Y, Stewart IT, Maurer EP. 2012. Development and application of a hydroclimatological stream temperature model within the Soil and Water Assessment Tool. *Water Resour Res* 48: WR01511.

Gay M, Okamura B, de Kinkelin P. 2001. Evidence that infectious stages of *Tetracapsula bryosalmonae* for rainbow trout *Oncorhynchus mykiss* are present throughout the year. *Dis Aquat Org* 46: 31–40.

Graham LP, Andréasson J, Carlsson B. 2007. Assessing climate change impacts on hydrology from an ensemble of regional climate models, model scales and linking methods – a case study on the Lule River basin. *Clim Change* 81: 293–307.

Hartikainen H, Johnes P, Moncrieff C, Okamura B. 2009. Bryozoan populations reflect nutrient enrichment and productivity gradients in rivers. *Freshw Biol* 54: 2320–2334.

Hutchins PR, Sepulveda AJ, Martin RM, Hopper LR. 2018. Improved conventional PCR assay for detecting *Tetracapsuloides bryosalmonae* DNA in fish tissues. *J Aquat Anim Health* 30: 164–170.

Klontz GW, Rourke AW, Eckblad W. 1986. The immune response during proliferative kidney disease in rainbow trout: a case history. *Vet Immunol Immunopathol* 12: 387–393.

Kristmundsson Á, Antonsson T, Árnason F. 2010. First record of Proliferative Kidney Disease in Iceland. *Bull Eur Assoc Fish Pathol* 30: 35–40.

Lauringson M, Nousiainen I, Kahar S, Burimski O, Gross R, Kaart T, Vasemägi A. 2021. Climate change-driven disease in sympatric hosts: temporal dynamics of parasite burden and proliferative kidney disease in wild brown trout and Atlantic salmon. *J Fish Dis* 44: 689–699.

Lauringson M, Ozerov M, Lopez M, Wennevik V, Niemelä E, Vorontsova T, Vasemägi A. 2022. Distribution and prevalence of the myxozoan parasite *Tetracapsuloides bryosalmonae* in northernmost Europe: analysis of three salmonid species. *Dis Aquat Org* 151: 37–49.

Lauringson M, Näslund J, Pukk L. et. al. Dams threaten salmonids by triggering temperature-dependent proliferative kidney disease. *Commun Biol* (2026). https://doi.org/10.1038/s42003-025-09470-1

Lewisch E, Unfer G, Pinter K, Bechter T, El-Matbouli M. 2018. Distribution and prevalence of T. bryosalmonae in Austria: a first survey of trout from rivers with a shrinking population. *J Fish Dis* 41: 1549–1557.

Li X, Anselin L. 2025. rgeoda: R Library for Spatial Data Analysis (Version 0.1.0) [Computer software]. https://cran.r-project.org/web/packages/rgeoda/index.html

Li X, Anselin L. 2021. rgeoda: R Library for Spatial Data Analysis (p. 0.1.0). https://doi.org/10.32614/CRAN.package.rgeoda

Lindeløv JK. 2024. mcp: Regression with Multiple Change Points (Version 0.3.4) https://cran.r-project.org/web/packages/mcp/index.html

Lindgren F, Rue H, Lindström J. 2011. An explicit link between Gaussian fields and Gaussian Markov random fields: The stochastic partial differential equation approach. *J Royal Stat Soc: Series B (Statistical Methodology)* 73: 423–498.

Lindgren F. 2023. fmesher: Triangle Meshes and Related Geometry Tools (p. 0.6.1) [Data set]. https://doi.org/10.32614/CRAN.package.fmesher

Lindström G, Johansson B, Persson M, Gardelin M, Bergström S. 1997. Development and test of the distributed HBV-96 hydrological model. *J Hydrol* 201: 272–288.

Lindström G, Pers C, Rosberg J, Strömqvist J, Arheimer B. 2010. Development and testing of the HYPE (Hydrological Predictions for the Environment) water quality model for different spatial scales. *Hydrol Res* 41: 295–319.

Macconnell E, Peterson JE. 1992. Proliferative kidney disease in feral cutthroat trout from a remote Montana reservoir: a first case. *J Aquat Anim Health* 4: 182–187.

Marcogliese DJ. 2008. The impact of climate change on the parasites and infectious diseases of aquatic animals. *Revue scientifique et technique/ Office international des epizooties* 27: 467–484.

Mayer PM, Reynolds SK, McCutchen MD, Canfield TJ. 2007. Meta-Analysis of nitrogen removal in riparian buffers. *J Environ Qual* 36: 1172–1180.

McCullough DA, Bartholow JM, Jager HI, Beschta RL, Cheslak EF, Deas ML, Ebersole JL, Foott JS, Johnson SL, Marine KR, Mesa MG, Petersen JH, Souchon Y, Tiffan KF, Wurtsbaugh WA. 2009. Research in thermal biology: burning questions for coldwater stream fishes. *Rev Fish Sci* 17: 90–115.

Mercier C, Duval E, Lefort M, Blanchet S, Veyssiere C, Loot G. 2025. Temporal Dynamics of a Fish Parasite (Tetracapsuloides bryosalmonae) and Its Two Main Hosts in Pyrenean Streams: An Environmental DNA-Based Approach. *Environ DNA* 7: e70127.

Mo TA, Jørgensen A. 2017. A survey of the distribution of the PKD-parasite *Tetracapsuloides bryosalmonae* (Cnidaria: Myxozoa: Malacosporea) in salmonids in Norwegian rivers—additional information gleaned from formerly collected fish. *J Fish Dis* 40: 621–627.

Moran PAP. 1950. Notes on continuous stochastic phenomena. *Biometrika* 37: 17–23.

Morris D, Ferguson H, Adams A. 2005. Severe, chronic proliferative kidney disease (PKD) induced in rainbow trout Oncorhynchus mykiss held at a constant 18 °C. *Dis Aquat Org* 66: 221–226.

Morris DJ, Adams A. 2006. Transmission of *Tetracapsuloides bryosalmonae* (Myxozoa: Malacosporea), the causative organism of salmonid proliferative kidney disease, to the freshwater bryozoan *Fredericella sultana*. *Parasitology* 133: 701–709.

Oexle S, Ros A, Brinker A. 2025. Evidence that wild salmonids seek cool water refuges to reduce parasite virulence: the proliferative kidney disease case. *Freshw Biol* 70(7): e70069.

Pebesma E, Bivand R, Racine E, Sumner M, Cook I, Keitt T, Lovelace R, Wickham H, Ooms J, Müller K, Pedersen TL, Baston D, Dunnington D. 2018. sf: Simple Features for R (Version 1.0-17) [Computer software]. https://cran.r-project.org/web/packages/sf/index.html

Pedersen TL. 2025. patchwork: The Composer of Plots (Version 1.3.1) [Computer software]. https://cran.r-project.org/web/packages/patchwork/index.html

Philpott D, Näslund J, Donadi S, Burimski O, Lauringson M, Pukk L, Vasemägi A. 2025. Effects of different preservatives during ecological monitoring of myxozoan parasite *Tetracapsuloides bryosalmonae* causing Proliferative kidney disease (PKD) in salmonids. *J Fish Dis* 48: e14095.

Raddum GG, Johnsen TM. 1983. Growth and feeding of *Fredericella sultana* (bryozoa) in the outlet of a humic acid lake. *Hydrobiologia* 101: 115–120.

Reid AJ, Carlson AK, Creed IF, Eliason EJ, Gell PA, Johnson PTJ, Kidd KA, MacCormack TJ, Olden JD, Ormerod SJ, Smol JP, Taylor WW, Tockner K, Vermaire JC, Dudgeon D, Cooke SJ. 2019. Emerging threats and persistent conservation challenges for freshwater biodiversity. *Biol Rev* 94: 849–873.

Ricciardi A, Reiswig HM. 1994. Taxonomy, distribution, and ecology of the freshwater bryozoans (Ectoprocta) of eastern Canada. *Can J Zool* 72: 339–359.

Rich B. 2023. table1: Tables of Descriptive Statistics in HTML (Version 1.4.3) [Computer software]. https://cran.r-project.org/web/packages/table1/index.html

Roberts RJ, Shepherd CJ. 1974. Handbook of trout and salmon diseases. Oxford, MA: Fishing News Books Ltd.

Ros A, Baer J, Basen T, Chucholl C, Schneider E, Teschner R, Brinker A. 2021. Current and projected impacts of the parasite *Tetracapsuloides bryosalmonae* (causative to proliferative kidney disease) on Central European salmonid populations under predicted climate change. *Freshw Biol* 66: 1182–1199.

Ros A, Schmidt-Posthaus H, Brinker A. 2022. Mitigating human impacts including climate change on proliferative kidney disease in salmonids of running waters. *J Fish Dis* 45: 497–521.

Rubin A, de Coulon P, Bailey C, Segner H, Wahli T, Rubin J-F. 2019. Keeping an eye on wild brown trout (*Salmo trutta*) populations: correlation between temperature, environmental parameters, and Proliferative kidney disease. *Front Vet Sci* 6: 281.

Saks L, Pukk L, Kahar S, Lauringson M, Vasemägi A. 2026. Rapid clearance of *Tetracapsuloides bryosalmonae* spores by freshwater sponge *Ephydatia muelleri*: potential implications for controlling proliferative kidney disease in salmonids. *J Fish Dis*, early online. https://doi.org/10.1111/jfd.70102

Schimanke S, Joelsson M, Andersson S, Carlund T, Wern L. 2022. Observerad klimatförändring i Sverige 1860–2021. Klimatologi 69. Norrköping: The Swedish Meteorological and Hydrological Institute (SMHI).

Schmidt-Posthaus H, Hirschi R, Schneider E. 2015. Proliferative kidney disease in brown trout: Infection level, pathology and mortality under field conditions. *Dis Aquat Org* 114: 139–146.

Schmidt-Posthaus H, Ros A, Hirschi R, Schneider E. 2017. Comparative study of proliferative kidney disease in grayling *Thymallus thymallus* and brown trout *Salmo trutta fario*: an exposure experiment. *Dis Aquat Org* 123: 193–203.

Schmidt-Posthaus H, Steiner P, Müller B, Casanova-Nakayama A. 2013. Complex interaction between proliferative kidney disease,

water temperature and concurrent nematode infection in brown trout. *Dis Aquat Org* 104: 23–34.

Seagrave CP, Bucke D, Hudson EB, McGregor D. 1981. A survey of the prevalence and distribution of proliferative kidney disease (PKD) in England and Wales. *J Fish Dis* 4: 437–439.

SLU. 2023. Miljödata-MVM [Data set]. Uppsala: Swedish University of Agricultural Sciences. https://miljodata.slu.se/MVM/Search

Solomon DJ, Lightfoot GW. 2008. The thermal biology of brown trout and Atlantic salmon. Science Report. Environment Agency, Rotherham.

Sterud E, Forseth T, Ugedal O, Poppe T, Jørgensen A, Bruheim T, Fjeldstad H, Mo T. 2007. Severe mortality in wild Atlantic salmon *Salmo salar* due to proliferative kidney disease (PKD) caused by *Tetracapsuloides bryosalmonae* (Myxozoa). *Dis Aquat Org* 77: 191–198.

Strepparava N, Ros A, Hartikainen H, Schmidt-Posthaus H, Wahli T, Segner H, Bailey C. 2020. Effects of parasite concentrations on infection dynamics and proliferative kidney disease pathogenesis in brown trout (*Salmo trutta*). *Transbound Emerg Dis* 67: 2642–2652.

Strepparava N, Segner H, Ros A, Hartikainen H, Schmidt-Posthaus H, Wahli T. 2018. Temperature-related parasite infection dynamics: the case of proliferative kidney disease of brown trout. *Parasitology* 145: 281–291.

Swedish Meteorological and Hydrological Institute (SMHI). 2025. SE.HY Delavrinningsområden (SVAR2022) (Version SVAR 2022:1.1) [Data set]. SMHI Open Data Catalog. https://opendata-catalog.smhi.se/md/90a1b29c-5a9f-4bc4-b26a-3d08611c0940

van Vliet MTH, Yearsley JR, Franssen WHP, Ludwig F, Haddeland I, Lettenmaier DP, Kabat P. 2012. Coupled daily streamflow and water temperature modelling in large river basins. *Hydrol Earth Syst Sci* 16: 4303–4321.

Wahli T, Bernet D, Segner H, Schmidt-Posthaus H. 2008. Role of altitude and water temperature as regulating factors for the geographical distribution of *Tetracapsuloides bryosalmonae* infected fishes in Switzerland. *J Fish Biol* 73: 2184–2197.

Wahli T, Knuesel R, Bernet D, Segner H, Pugovkin D, Burkhardt-Holm P, Escher M, Schmidt-Posthaus H. 2002. Proliferative kidney disease in Switzerland: current state of knowledge. *J Fish Dis* 25: 491–500.

Waldner K, Borkovec M, Borgwardt F, Unfer G, El-Matbouli M. 2021. Effect of water temperature on the morbidity of *Tetracapsuloides bryosalmonae* (Myxozoa) to brown trout (*Salmo trutta*) under laboratory conditions. *J Fish Dis* 44: 1005–1013.

Wanders N, Van Vliet MTH, Wada Y, Bierkens MFP, Van Beek LPH. (Rens). 2019. High-resolution global water temperature modeling. *Water Resour Res* 55: 2760–2778.

Wang Z, Pu D, Zheng J, Li P, Lü H, Wei X, Li M, Li D, Gao L. 2023. Hypoxia-induced physiological responses in fish: From organism to tissue to molecular levels. *Ecotoxicol Environ Safety* 267: 115609.

Wickham H, Averick M, Bryan J, Chang W, McGowan LD, François R, Grolemund G, Hayes A, Henry L, Hester J, Kuhn M, Pedersen TL, Miller E, Bache SM, Müller K, Ooms J, Robinson D, Seidel DP, Spinu V, Yutani H. 2019. Welcome to the Tidyverse. *J Open Source Softw* 4(43): 1686.

Zaidel PA, Roy AH, Houle KM, Lambert B, Letcher BH, Nislow KH, Smith C. 2021. Impacts of small dams on stream temperature. *Ecol Indic* 120: 106878.

Zeileis A, Grothendieck G, Ryan JA, Ulrich JM, Andrews F. 2025. zoo: S3 Infrastructure for Regular and Irregular Time Series (Z's Ordered Observations) (Version 1.8-14) [Computer software]. https://cran.r-project.org/web/packages/zoo/index.html

Cite this article as: Philpott D, Näslund J, Donadi S, Lindmark M, Vasemägi A. 2026. Large-scale spatial analyses reveal hotspots of proliferative kidney disease in brown trout and interactive effects of temperature and parasite load. *Knowl. Manag. Aquat. Ecosyst.*, 427: 8. https://doi.org/10.1051/kmae/2026002